Field-induced patterns in confined magnetorheological fluids

Sérgio A. Lira and José A. Miranda*
Departamento de Física, LFTC, Universidade Federal de Pernambuco, Recife 50670-901, PE, Brazil

Rafael M. Oliveira
Department of Mechanical Engineering, University of California, Santa Barbara, California 93106, USA
(Received 6 October 2009; published 7 April 2010)

We study the behavior of a magnetorheological fluid droplet confined to a Hele-Shaw cell in the presence of an applied radial magnetic field. Interfacial pattern formation is investigated by considering the competition among capillary, viscoelastic, and magnetic forces. The contribution of a magnetic field-dependent yield stress is taken into account. Linear stability analysis reveals the stabilizing role played by yield stress. On the other hand, a mode-coupling approach predicts that the resulting fingering structures should become less and less sharp as yield stress effects are increased. By employing a vortex-sheet formalism we have been able to identify a family of exact stationary solutions of the problem, unveiling the development of swollen polygonal patterns. A suggestive magnetically controlled shape transition in which the edges of the patterns change from convex to concave has been also identified.

DOI: 10.1103/PhysRevE.81.046303 PACS number(s): 47.54.−r, 47.15.gp, 47.65.Cb, 83.60.La

I. INTRODUCTION

Magnetic fluids, termed as ferrofluids [1,2], are stable colloidal suspensions typically containing water or oil combined with nanometersized magnetic particles. This particular type of magnetic fluid is ultrastable against settling, behaves superparamagnetically, and is characterized by its prompt response to even modest magnetic fields. Due to its responsiveness to magnetic stimuli, the study of ferrofluid interfacial pattern formation has become considerably popular [3,4]. In particular, under spatially confined circumstances of a Hele-Shaw cell the viscosity-driven Saffman-Taylor instability [5] is supplemented by a magnetically induced instability, leading to a variety of interesting interfacial behaviors. The Hele-Shaw flow problem, with either nonmagnetic or magnetic fluids, has already proven its prototypical role in the context of interfacial pattern formation [6].

One compelling example of pattern-forming systems in confined ferrofluids is related to the labyrinthine instability [7–9], in which highly branched structures are formed when a magnetic field is applied perpendicularly to the plates of a Hele-Shaw cell. Beautiful spiral patterns and amazing protozoanlike shapes can also arise when a rotating magnetic field is added to the perpendicular field setup [10]. The emergence of peculiar diamond-ring-shaped structures has been detected in centrifugally driven Hele-Shaw flows under the action of an azimuthal magnetic field [11]. In addition, quite regular n-fold symmetric shapes emerge in both immiscible [12] and miscible [13] ferrofluids when perpendicular and azimuthal magnetic fields are applied simultaneously. Finally, the development of starfishlike morphologies has been recently predicted if a radial magnetic field configuration is used [14].

In contrast to what happens to ferrofluids, the investigation of Hele-Shaw pattern formation with magnetorheological (MR) fluids has been amply overlooked. Magnetorheological fluids consist of much larger, micronsized magnetized particles dispersed in aqueous, or organic carrier liquids. The unique feature of this kind of magnetic fluid is the abrupt change in its viscoelastic properties upon the application of an external magnetic field [15–19]. In the absence of an applied field ("off" state) the magnetized particles in the suspension are randomly distributed, so that MR fluids appear similar to usual nonmagnetic fluids. However, when a magnetic field is applied ("on" state) the large particles suspended in the fluid interact, and tend to align and link together along the field's direction, creating long particle chains, columns, and other more complex structures. Interestingly, the formation of such structures restrict the motion of the fluid, allowing it to display a solidlike behavior.

A MR fluid can be characterized by its yield stress, which measures the strength of the field-induced structures formed. As opposed to Newtonian fluids, yield stress fluids [20] (magnetic or not) can support shear stresses without flowing. As long as the stress remains below to a certain critical value they do not flow, but respond elastically to deformation. In MR fluids the yield stress is magnetic field-dependent, and varies quadratically with the strength of the applied field. As the magnitude of the applied magnetic field is increased, the yield stress which is associated to the highest value of stress required to break the existing network of magnetic interactions, also increases. In this sense, MR fluids work as smart materials whose viscoelastic properties can be conveniently tuned by an applied magnetic field. By the way, the appearance of viscoelastic properties such as yield stress in ferrofluids, and its quadratic dependence on the applied magnetic field has been recently verified experimentally [21,22]. Nevertheless, it has been found that in ferrofluids the field-dependent yield stress is indeed very small as compared to the typical values obtained for MR fluids.

In this work we embark upon the study of pattern formation phenomena in MR fluids confined in Hele-Shaw geometry. Considering the paradigmatic role played by Hele-Shaw flows [1–6], our investigation can be of significance to a

*jme@df.ufpe.br

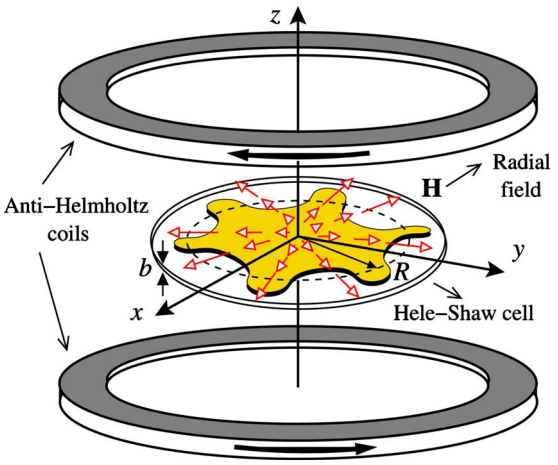

FIG. 1. (Color online) Schematic illustration of a Hele-Shaw cell of thickness b containing an initially circular droplet (dashed curve) of a MR fluid, surrounded by a nonmagnetic fluid. The anti-Helmholtz coils produce a magnetic field $\mathbf{H}$ pointing radially outwards in the plane of the cell. Fingering interfacial patterns arise due to the action of the radial magnetic field.

number of physical, biological, and engineering systems related to the viscous fingering phenomenon. It is in this context where the problem we study can gain some more general relevance. We follow a previous analysis recently performed by our research group [14] in which the response of a *ferrofluid* droplet to a radial magnetic field has been investigated. Here, unlike most common situations examined in the literature, we focus on the situation where the constrained drop is a *magnetorheological* fluid, allowing its yield stress to be manipulated via the application of an external radial magnetic field. The magnetically tuned viscoelastic properties introduced by this system open up the possibility of unveiling still unexplored pattern morphologies and interesting dynamic behavior.

In Sec. II, the basic equations describing the system are presented, and the moving boundary problem is properly specified. By employing a mode-coupling approach (Sec. III) we have been able to study the linear stability of the rising patterns, as well as to examine important aspects of their morphology at the onset of nonlinear effects. A more detailed account of the resulting nonlinear shapes is provided by the determination of nontrivial exact stationary solutions for the problem with nonzero surface tension. These solutions are obtained through a vortex-sheet formalism, and reveal the development of characteristic swollen polygon-shaped patterns (Sec. IV). We have also identified a magnetically induced shape transition in which the interface goes from convex to concave as magnetic field effects are considerably larger than interfacial tension. A summary of our chief conclusions is presented in Sec. V.

II. PHYSICAL PROBLEM AND GOVERNING EQUATIONS

Figure 1 illustrates an incompressible, MR fluid droplet of unperturbed radius R and viscosity η, which is surrounded by a nonmagnetic, Newtonian fluid of negligible viscosity. The fluids are located between two narrowly spaced flat plates of a Hele-Shaw cell of thickness b. The surface tension between the fluids is nonzero and denoted by γ. We consider that the MR fluid droplet is subjected to an in-plane radial magnetic field

$$\mathbf{H} = \frac{H_0}{L} r\hat{\mathbf{r}}, \tag{1}$$

where r is the radial distance from the origin of the coordinate system (located at the center of the droplet), H_0 is a constant, L is a characteristic length, and $\hat{\mathbf{r}}$ is a unit vector in the radial direction. It is worth pointing out that this specific magnetic field configuration can be generated by a pair of identical Helmholtz coils whose currents are equal and flow in opposite directions ("anti-Helmholtz" configuration). The experimental conditions required to obtain such a radial magnetic field have been discussed in detail in [23].

For the quasi-two-dimensional geometry of the Hele-Shaw cell, one reduces the three-dimensional flow to an equivalent two-dimensional one by averaging the Navier-Stokes equation over the direction perpendicular to the plates. The gap-average procedure is performed by neglecting the inertial terms, considering a large aspect ratio geometry ($R \gg b$), and using the Bingham model for yield stress fluids [24,25]. By taking into account the contribution of viscoelastic and magnetic effects, plus the existence of a magnetic field-dependent yield stress $\sigma_y = \sigma_y(H)$, one can write a modified Darcy's law for the gap-averaged velocity $\mathbf{v}$ of a confined MR fluid [24–26]

$$\mathbf{v} = -\frac{b^2}{12\eta}\left[\boldsymbol{\nabla}\Pi + \frac{3\sigma_y(H)}{b}\hat{\mathbf{r}}\right]. \tag{2}$$

The derivation of Eq. (2) assumes the regime of high viscosity compared to yield effects. On the basis of the symmetry of the applied magnetic field configuration, we consider the prevalent yielding occurring along the radial direction. Note that one recovers the usual Darcy's law for Newtonian magnetic fluids [7,8] by setting $\sigma_y(H)=0$.

The gap-averaged generalized pressure is defined as

$$\Pi = \frac{1}{b}\int_{-b/2}^{+b/2} [P - \Psi] dz, \tag{3}$$

where P is the three-dimensional hydrodynamic pressure,

$$\Psi = \mu_0 \int_0^H M dH \tag{4}$$

represents a magnetic pressure, μ_0 denotes the magnetic permeability of free space, and M is the magnetization of the MR fluid. Note that for the nonmagnetic fluid $M=0$. In this context, the magnetic body force acting on the MR fluid is given by $\mu_0 M \boldsymbol{\nabla} H$ [1,2], where H is the applied magnetic field.

The magnetic field-dependent yield stress is given by [17–19,21,22,27,28]

$$\sigma_y(H) = \sigma_{y0} + \alpha H^2, \tag{5}$$

where σ_{y0} represents the yield stress in the absence of the magnetic field, and α is a constant that depends on the material properties of the MR fluid, being proportional to the particle volume fraction [19]. In general the field dependence of a yield stress fluid is represented by a power law $\sigma_y(H) - \sigma_{y0} \sim H^n$ with $1 \leq n \leq 2$, and the case we consider here $n=2$ is the one for which the magnetization is linearly related to the applied magnetic field [17–19] $\mathbf{M} = \chi \mathbf{H}$, where χ is the magnetic susceptibility. This linear relation holds as long as $H \ll H_{sat}$, where H_{sat} is the field magnitude at saturation magnetization [$O(10^2$ kA/m-10^3 kA/m)]. It is worth emphasizing that, despite the non-Newtonian character of the MR fluid (due to its yield stress), we consider that it presents a constant viscosity. This assumption enables the flow to stay potential. Of course, more involved theoretical descriptions may incorporate a shear and magnetic field-dependent viscosity to certain types of magnetic fluids [29], but this is beyond the scope of our current work.

Forces arising from gradients of the mean pressure, as in the case of Darcy's law Eq. (2), characterize an irrotational flow in the bulk. In this framework Darcy's law Eq. (2) can be conveniently rewritten in a *dimensionless* form

$$\mathbf{v} = -\nabla \phi,$$

$$\phi = p - \chi N_B r^2 + S_0 r + S r^3, \tag{6}$$

where ϕ is a velocity potential, and p is the gap-averaged hydrodynamic pressure. The parameter

$$N_B = \frac{\mu_0 H_0^2 r_0^3}{2\gamma L^2} \tag{7}$$

represents the dimensionless magnetic Bond number, and measures the ratio of magnetic to capillary forces. In addition

$$S_0 = \frac{3\sigma_{y0} r_0^2}{\gamma b} \tag{8}$$

and

$$S = \frac{\alpha H_0^2 r_0^4}{\gamma L^2 b} \tag{9}$$

are related to the yield-stress contributions at zero, and nonzero applied magnetic field, respectively. In Eq. (6) lengths and velocities are rescaled by r_0, and $\gamma b^2/(12\eta r_0^2)$, respectively. The typical length scale r_0 is of the order of the unperturbed droplet radius R, and will be more properly defined subsequently (Sec. IV). From now on, we work with the dimensionless version of the equations.

By inspecting Eq. (6) the driving and stabilizing forces of the problem become apparent. It has a radial driving force pushing the MR fluid off center, with a term growing linearly with the radial coordinate (proportional to N_B) stemming from the magnetic pressure Eq. (4). Moreover, it presents two stabilizing contributions, the first one being a constant force (proportional to S_0), and a second which is quadratic (proportional to S) in the radial coordinate. These stabilizing forces come from the two terms of the yield stress given by Eq. (5). Already at this point, we can find noteworthy connections of Eq. (6) with general Hele-Shaw flow problems: one can identify the rotating Hele-Shaw centrifugal force [30–32], and the channel-geometry constant driving force (gravity or pressure difference) [33,34] but of stabilizing nature. On the other hand, the quadratic term in the force (proportional to S) is unparalleled, being exclusively related to the field-dependent yield stress.

Further specification about the velocity potential is provided by the augmented pressure jump boundary condition

$$\Delta p = \kappa - N_B \chi^2 r^2 (\hat{\mathbf{n}} \cdot \hat{\mathbf{r}})^2, \tag{10}$$

where $\hat{\mathbf{n}}$ denotes the unit normal vector to the interface. The first term on the right-hand side of Eq. (10) represents the usual contribution related to surface tension and interfacial curvature κ. Here κ is the dimensionless in-plane curvature. The meniscus curvature, in the direction perpendicular to the plates, is of larger magnitude, but nearly constant. Therefore, its gradient is nearly zero, so that it does not significantly affect the dynamics. When the assumption of constant meniscus curvature is valid, the cell gap thickness can be scaled out of the problem, since it always appears together with the viscosity. This is the reason why the basic equations of the problem are not explicitly dependent on b. The second term in Eq. (10) is set by the so-called magnetic normal traction [1,2], which considers the influence of the normal component of the magnetization at the interface, and its linear relation to the applied magnetic field.

From the incompressibility condition $\nabla \cdot \mathbf{v} = 0$ it can be verified that the velocity potential is Laplacian. Therefore, the definition of the moving boundary problem is specified by the following equations

$$\nabla^2 \phi = 0, \tag{11}$$

$$\left.\frac{\partial \phi}{\partial n}\right|_{in} = \left.\frac{\partial \phi}{\partial n}\right|_{out}, \tag{12}$$

$$\left.\frac{\partial \phi}{\partial s}\right|_{in} - \left.\frac{\partial \phi}{\partial s}\right|_{out} = \Gamma, \tag{13}$$

where the subscripts label the inner (*in*) and outer (*out*) fluids, and $\partial/\partial s = \partial_s$ ($\partial/\partial n = \partial_n$) is the derivative along the tangent (normal) direction to the interface. Equation (12) describes the continuity of the normal velocity at the interface, and Eq. (13) its tangential jump of magnitude Γ. This jump originates a nonzero vorticity region restricted to the interface separating the fluids [35,36]. With the help of the generalized Darcy's law Eq. (6), and the pressure jump Eq. (10) an explicit expression for the vortex sheet strength can be derived yielding

$$\Gamma = 2\partial_s \{\kappa - N_B r^2 \chi [1 + \chi (\hat{\mathbf{n}} \cdot \hat{\mathbf{r}})^2] + S_0 r + S r^3\} - \left(\left.\frac{\partial \phi}{\partial s}\right|_{in} + \left.\frac{\partial \phi}{\partial s}\right|_{out} \right). \tag{14}$$

While presenting our results in Secs. III and IV we make sure that the values of all relevant dimensionless quantities

we utilize [Eqs. (7)–(9)] are consistent with realistic physical parameters related to existing magnetic field arrangements, and material properties of MR fluids. For the typical parameters related to the Hele-Shaw setup under study, we take $b=10^{-3}$ m (which appears in S_0 and S), and $R=10^{-2}-10^{-1}$ m. Recall that r_0 (that shows up in N_B, S_0, and S) has the same order of magnitude of R. While dealing with the strength of the magnetic fields, we consider relatively low values $2.5\ \mathrm{kA/m} \leq H_0 \leq 10\ \mathrm{kA/m}$ which are easily achievable by using a typical Helmholtz coils setup, where the radius of a coil is considerably larger than the radius of the MR fluid droplet. The characteristic length L related to the radial magnetic configuration is of the order of a few centimeters [23]. The quantities H_0 and L are present in the parameters N_B and S. Regarding the material properties of the MR fluid, in S we take $\alpha=3.0\times10^{-7}$ $\mathrm{N/A^2}$ [21,28], and in S_0 consider that the "off" state yield stress σ_{y0} varies from 0.3 Pa to 45 Pa [28,37]. For the magnetic susceptibility we take $0.1 \leq \chi \leq 1$ [38]. Finally, for the surface tension γ we use a typical value of 10^{-3} Pa m in the parameters given by Eqs. (7)–(9).

III. LINEAR STABILITY AND WEAKLY NONLINEAR DYNAMICS

After having formally stated the moving boundary problem in terms of the velocity potential, we proceed by employing a perturbative mode-coupling approach to examine the linear stability of the interface, and morphological features of the resulting patterns at the onset of nonlinear effects.

Due to the action of the radial magnetic field the fluid-fluid interface may deform, and its perturbed shape is described as $\mathcal{R}(\varphi,t)=R+\zeta(\varphi,t)$, where $\zeta(\varphi,t)=\Sigma_{n=-\infty}^{+\infty}\zeta_n(t)\exp(in\varphi)$ represents the net interface perturbation with Fourier amplitudes $\zeta_n(t)$, and discrete azimuthal wave numbers n. The azimuthal angle in the plane of the Hele-Shaw cell is denoted by φ. We define Fourier expansions for the velocity potential, and use the boundary conditions presented in Sec. II to express ϕ in terms of ζ_n to obtain a dimensionless mode-coupling differential equation for the system (for $n\neq0$), accurate to second-order in the perturbation amplitudes

$$\frac{d\zeta_n}{dt} = \lambda(n)\zeta_n + \sum_{n'\neq0} [F(n,n') + \lambda(n')G(n,n')]\zeta_{n'}\zeta_{n-n'}, \tag{15}$$

where

$$\lambda(n) = |n|\left[2N_B\chi(1+\chi) - \frac{1}{R^3}(n^2-1) - \frac{S_0}{R} - 3SR\right] \tag{16}$$

is the linear growth rate. The second-order mode-coupling terms are represented as

$$F(n,n') = \frac{|n|}{R}\left\{N_B\chi\{1+\chi[1+n'(n-n')]\} - \frac{1}{R^3}\left[1-\frac{n'}{2}(3n'+n)\right] - 3SR\right\}, \tag{17}$$

$$G(n,n') = \frac{1}{R}\{|n|[\mathrm{sgn}(nn')-1]-1\}. \tag{18}$$

The sign function sgn equals ±1 according to the sign of its argument. Notice that when $S=S_0=0$ Eqs. (16)–(18) reproduce the results obtained in [14] for the corresponding problem in Newtonian ferrofluids, where yield stress effects have been completely neglected.

The terms appearing in the expression for the function $F(n,n')$ in Eq. (17) arise from the magnetic applied field, surface tension, and field-dependent yield stress, respectively. The term proportional to χ^2 comes from the square of the projection of the interface normal in the radial direction in the pressure jump condition [Eq. (10)]. In contrast the function $G(n,n')$ defined in Eq. (18) presents no dependence on magnetic effects.

We use Eq. (15) to investigate how the development of interfacial instabilities at early stages of the pattern formation is influenced by the radial magnetic field. At the linear level, the relevant physical effects examined in the discussion of Eq. (6) just add up, as expressed by the linear growth rate. Since a positive $\lambda(n)$ leads to an unstable interface, Eq. (16) tells us that for a given nonzero χ, N_B destabilizes the system. As expected, the magnetic contribution to the growth rate tends to move the MR fluid toward regions of higher magnetic fields, stimulating the growth of fingering structures. This behavior is analogous to the role played by the centrifugal force in the rotating Hele-Shaw problem [30–32]. On the other hand, the term involving (n^2-1) is associated to the surface tension and plays a stabilizing role. The terms related to the yield stress contribution (S and S_0) are also stabilizing and tend to inhibit fingering formation. In particular the term S_0 is related to a constant radial force acting similarly to gravity or pressure difference appearing in the usual Saffman-Taylor problem in channel geometry [33,34].

By examining Eq. (16) it is evident that increasingly larger values of S and S_0 shrink the band of unstable modes [which can be accessed by taking $\lambda(n)=0$]. In addition, we notice that the maximum of $\lambda(n)$ which occurs at $n=n_{max}$, where

$$n_{max} = \sqrt{\frac{1}{3}\left\{1+R^3\left[2N_B\chi(1+\chi) - \frac{S_0}{R} - 3SR\right]\right\}} \tag{19}$$

decreases as S or S_0 is ramped up. As it is well known, the fastest growing mode, given by the closest integer to n_{max}, is the mode that will tend to dominate during early stages of the pattern formation.

In summary, at the very early stages of the dynamics the role of the yield stress terms is to decrease the wave number of maximum growth just as the maximum growth rate, and to tight the band of unstable modes. Conversely, both N_B and χ tend to destabilize the system. Note that the additional magnetization term appearing in Eq. (10) is of second order in the interface perturbation ζ, being legitimately nonlinear and therefore of no influence at purely linear stages of interfacial evolution.

Despite the importance of the linear stability analysis, interesting information about the morphology of the rising patterns can be acquired at the weakly nonlinear stage of the interface evolution. We investigate how the radial magnetic field influences the shape of the emerging MR fluid patterns by using the full mode-coupling differential Eq. (15). As in [14,39], we study a mechanism controlling the finger shape behavior through magnetic means, and consider the coupling of a small number of modes. To simplify our discussion we rewrite Eq. (15) in terms of cosine and sine modes, where the cosine $a_n=\zeta_n+\zeta_{-n}$ and sine $b_n=i(\zeta_n-\zeta_{-n})$ amplitudes are real-valued. Without loss of generality we choose the phase of the fundamental mode so that $a_n>0$ and $b_n=0$. Under such circumstances, finger tip-sharpening and tip-broadening phenomena are described by considering the influence of a fundamental mode n on the growth of its harmonic $2n$. One key piece of information about the morphology of the emerging patterns can be extracted from the equation of motion for the harmonic cosine mode

$$\frac{da_{2n}}{dt}=\lambda(2n)a_{2n}+\frac{1}{2}T(2n,n)a_n^2, \tag{20}$$

where the finger tip function is defined as

$$T(2n,n)=[F(2n,n)+\lambda(n)G(2n,n)]. \tag{21}$$

It can be shown that the equivalent growth of the sine mode b_{2n} is uninfluenced by a_n and does not present second-order couplings, so we focus on the growth of the cosine mode.

The interesting point about the function $T(2n,n)$ is that it controls the finger shape behavior. The sign of $T(2n,n)$ dictates whether finger tip-sharpening or finger tip broadening is favored by the dynamics. From Eq. (20) we see that if $T(2n,n)>0$, the result is a driving term of order a_n^2 forcing growth of $a_{2n}>0$, the sign that is required to cause outward-pointing fingers to become sharp, favoring finger tip sharpening. In contrast, if $T(2n,n)<0$ growth of $a_{2n}<0$ would be favored, leading to outwards-pointing finger tip broadening.

In order to gain insight about the morphological response of the fingers to the action of a radial magnetic field, and also to the effects induced by yield stress, in Fig. 2 we plot $T(2n,n)$ as a function of N_B. We consider two distinct values of S_0, and for each one of them we take three increasingly larger values of S. As in [14], to ensure that both participating modes (n and $2n$) are able to grow we take n such that $\lambda(2n)=0$, implying in the observance of a critical value of N_B for each pair of S_0 and S.

By inspecting Fig. 2 we readily observe that $T(2n,n)$ is a positive, increasing function of N_B, indicating that once the fingers are formed they tend to develop sharp tips. Moreover, for a given S_0 we notice that $T(2n,n)$ tends to decrease as one increases the value of S. This indicates that the yield stress influences the shape of the patterns, inhibiting the formation of pronounced spiked tips. It is also clear that larger values of S_0 favor further suppression of sharp edged fingers.

We conclude this section by contrasting the finger tip behavior studied here with other general Hele-Shaw problems. First, we point out that in the channel geometry Hele-Shaw setup [33,34] there is no coupling between the fundamental and its first harmonic mode, leading to absence of finger tip splitting at second order. Besides, the situation of a Newtonian ferrofluid in the presence of a radial magnetic field [14] does present such a coupling, resulting in a high magnitude, positive finger tip function $T(2n,n)$ which favors the formation of sharp fingers. However, in the MR fluid case, the presence of the yield stress (negative sign) terms S and S_0 in the mode-coupling function $F(n,n')$ and in $\lambda(n)$ conspire to produce a positive finger tip function of smaller magnitude, resulting in fingering structures that are less sharp than the ones obtained with Newtonian ferrofluids.

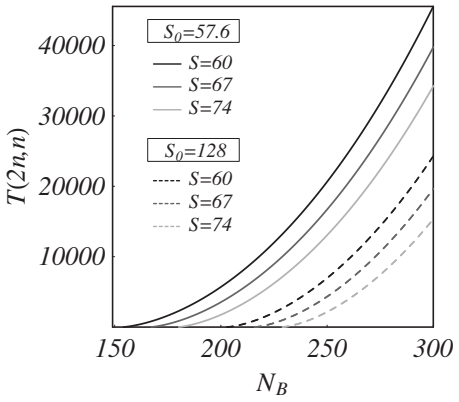

FIG. 2. Behavior of the finger tip function $T(2n,n)$ as the magnetic Bond number N_B is varied, for $R=0.9$, $\chi=0.5$, and two different values of the zero field yield stress parameter: $S_0=57.6$ (solid curves), and $S_0=128$ (dashed curves). For each value of S_0, three increasing magnitudes for the magnetic field-dependent yield stress parameter are used: $S=60$ (black), $S=67$ (dark gray), and $S=74$ (light gray).

The weakly nonlinear predictions suggest that the resulting fingers should become less and less sharp as the yield stress parameters are augmented. In this sense, our mode-coupling approach enables one to access analytically the morphology of the emerging structures already at very early nonlinear stages of the dynamics. This is in contrast to the usual purely linear results which primarily refer to the stability of the patterns.

IV. EXACT STATIONARY SOLUTIONS

In this section we turn to a more specific description of the patterns' morphology through the calculation of exact solutions for this problem. The exact stationary solutions reveal even more details about the shape of the patterns. Similarly to [14] we apply a vortex-sheet formalism [35,36] in order to access the exact stationary shapes obtained when a droplet of a confined MR fluid is subjected to a radial magnetic field. As discussed in detail in [40,41] this type of exact solutions with nonzero surface tension can be found by imposing a condition of zero vorticity ($\Gamma=0$) plus considering a stationary state ($\partial\phi/\partial s|_{in}=\partial\phi/\partial s|_{out}=0$) in Eq. (14). Under such circumstances, we find that the curvature of the interface satisfies a nonlinear ordinary differential equation

$$\partial_s\{\kappa-N_Br^2\chi[1+\chi(\hat{\mathbf{n}}\cdot\hat{\mathbf{r}})^2]+S_0r+Sr^3\}=0, \tag{22}$$

which can be integrated to obtain

$$\kappa = \kappa(r, r \sin \psi) = a + br^2 + c(r \sin \psi)^2 - S_0 r - Sr^3, \tag{23}$$

where a is a constant of integration. For brevity we define $b=N_B\chi$, and $c=N_B\chi^2$. In Eq. (23) we have used the fact that $\hat{\mathbf{n}}\cdot\hat{\mathbf{r}} = \pm \sin \psi$, where ψ is the angle between the radius vector $\hat{\mathbf{r}}$ and the tangent vector $\hat{\mathbf{s}}$ at the interface.

Our goal is to study the fully nonlinear family of planar curves whose curvature has the general form given by Eq. (23). These curves are the nonzero surface tension exact stationary solutions which balance the competing capillary, viscoelastic, and magnetic effects at the MR fluid interface. A number of important morphological features of the stationary solutions can be obtained by the numerical evaluation of the nonlinear differential Eq. (22), without recourse to intensive numerical simulations. This way, we can explore the richness behind a family of curves whose curvatures are prescribed by Eq. (23) by manipulating the relevant control parameters of the problem, namely, N_B, χ, S_0, S, the constant a, and the specifications $r_0=r(\varphi=0)$ and $\psi_0=\psi(\varphi=0)$. For a thorough discussion about the numerical approach used to solve the type of differential equation given in Eq. (22) we refer the reader to [41].

The parameter r_0 defines the maximum radial distance obtained for a given stationary pattern. At this point, we justify our choice of r_0 as a convenient parameter to rescale lengths in our problem. If the unperturbed radius R were to be chosen as the parameter to rescale lengths, a very strict constraint would be imposed to the system, since in this case all the areas of the resulting exact steady shapes should have to coincide. It turns out that it is not at all trivial to keep the areas of all perturbed patterns the same, and simultaneously fulfill the requirements that all interfacial curves should be closed (i.e., commensurable with 2π), and non-self-intersecting. We have circumvented this practical difficulty by conveniently selecting r_0 as the appropriate length scale for the problem without loss of generality.

In Fig. 3, we present a representative collection of possible exact stationary solutions for the problem of a confined MR fluid droplet under the influence of a radial magnetic field. The shapes are obtained for $N_B=256$, $\chi=0.5$, $\psi_0=\pi/2$, $r_0=1$, $S_0=57.6$, and by considering four decreasing values of the magnetic field-dependent yield stress parameter S: (a) 105.13, (b) 100.13, (c) 93.13, and (d) 84.13. For convenience, for each value of S, we adjust the constant a so that the final pattern has the number of fingers (or, edges) $n=n_{max}$ as arising from the linear regime according to Eq. (19). We emphasize that the choice of a is arbitrary, and the way we set it should not be interpreted as if the linear regime dictates the final morphological features of the fully nonlinear exact steady shapes. Note that all patterns shown in this work are stationary shapes, and *not* a time evolving sequence of events. The resulting peculiar shapes depicted in Fig. 3 resemble convex-shaped polygons. In fact, they are what we could name as n-gons with $n=2$, 3, 4 and 5 corners. They look like "swollen" regular polygons presenting convex edges. This family of shapes differs from the ones obtained in [14] for Newtonian ferrofluids, where concave-shaped polygons and peaky starfishlike structures (with edges curved inward) have been obtained. So, the convex-shape signature of the patterns can be attributed to the yield stress effects introduced by the parameters S_0 and S. It is also evident from Fig. 3 that by decreasing the value of S (keeping N_B and S_0 fixed) the number of fingering structures (or, corners) increases.

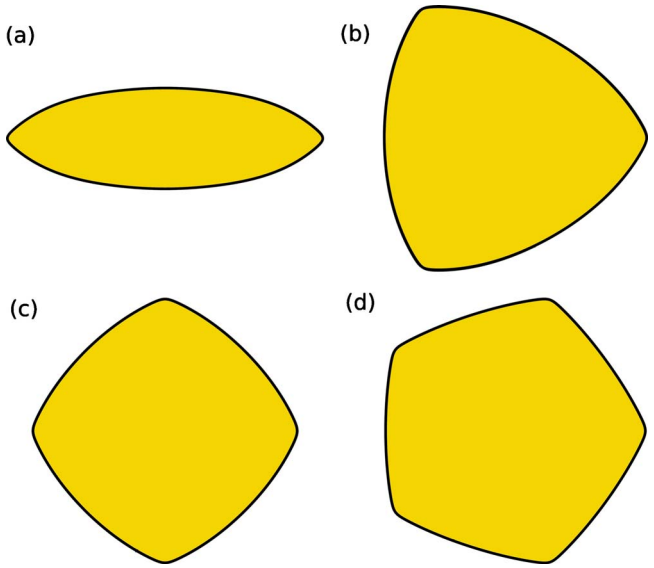

FIG. 3. (Color online) Typical stationary shape solutions for $N_B=256$, $\chi=0.5$, $\psi_0=\pi/2$, $r_0=1$, $S_0=57.6$, and (a) $S=105.13$, (b) $S=100.13$, (c) $S=93.13$, and (d) $S=84.13$.

Figure 4 addresses a situation similar to the one illustrated in Fig. 3, but now taking a larger value of the zero applied field yield stress parameter $S_0=128$. We set $N_B=256$, $\chi=0.5$, $\psi_0=\pi/2$, $r_0=1$, and consider the following decreasing values of S: (a) 81.67, (b) 76.67, (c) 69.67, and (d) 60.67. As

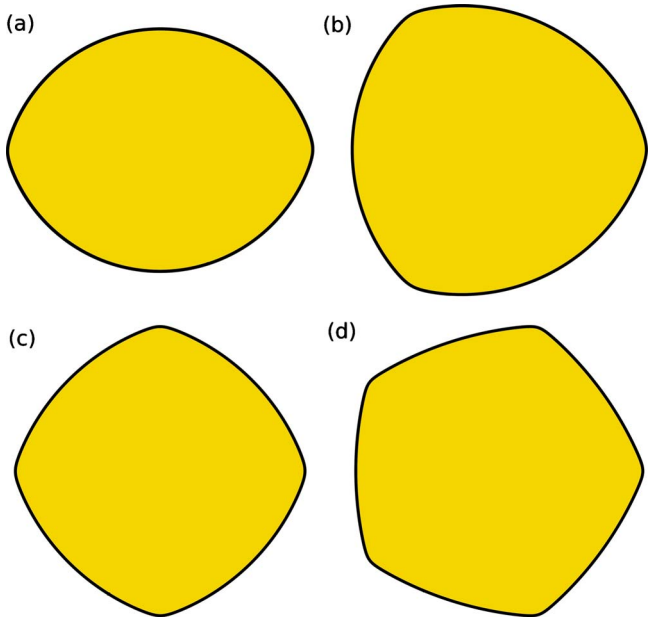

FIG. 4. (Color online) Typical stationary shape solutions for $N_B=256$, $\chi=0.5$, $\psi_0=\pi/2$, $r_0=1$, $S_0=128$, and (a) $S=81.67$, (b) $S=76.67$, (c) $S=69.67$, and (d) $S=60.67$.

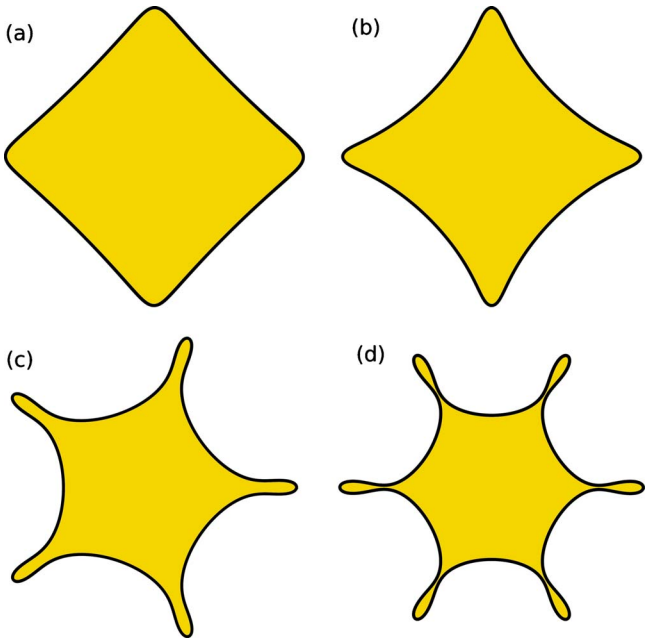

FIG. 5. (Color online) Gallery of possible patterns for increasingly larger values of the magnetic Bond number N_B. It is assumed that $\chi=0.5$, $\psi_0=\pi/2$, $r_0=1$, $a=-6.36$, $S_0=38.02$, $S=23.80$, and (a) $N_B=109.85$, (b) $N_B=126.57$, (c) $N_B=148.06$, and (d) $N_B=150.53$.

in Fig. 3 for each value of S we adjust the magnitude of a so that $n=n_{max}$. The resulting exact shapes are again characterized as regular n-gons presenting convex-shaped edges, where the number of corners increase for lower values of S. However, the patterns shown in Fig. 4 for $S_0=128$, are even more "inflated" than the ones obtained in Fig. 3 for $S_0=57.6$. In Fig. 4 the edges bulge outward, making the tips of the fingers to become not as sharp as the ones obtained in Fig. 3. In other words, the consideration of larger values of S_0 resulted in the inhibition of sharper tips. The comparison between the characteristic shapes presented in Figs. 3 and 4 reinforces the validity of the weakly nonlinear predictions made in Sec. III, which prognosticated diminished tendency toward finger tip-sharpening for larger S_0.

Another situation of interest refers to the response of the patterns to increased values of the magnetic Bond number N_B. This issue is investigated in Fig. 5. It depicts interfacial MR fluid patterns generated by taking $\chi=0.5$, $\psi_0=\pi/2$, $r_0=1$, $a=-6.36$, $S_0=38.02$, $S=23.80$, and four increasingly larger magnitudes of N_B: (a) 109.85, (b) 126.57, (c) 148.06, and (d) 150.53. Instead of plain convex-shaped structures, different types of patterns arise as N_B increases: first, in Fig. 5(a) a nearly perfect square with almost straight edges is observed. Therefore, the convex polygon sides obtained in Figs. 3 and 4 have flattened out. As N_B increases further [Fig. 5(b)] a sort of "shape transition" is revealed, showing the appearance of a concave-shaped four-gon presenting more pointy corners (or, fingers). If N_B continues to increase [Fig. 5(c)] the number of fingers also increases, while protrusions start growing from them leading to the formation of a starfish-like pattern presenting 5 fingers, similar to those observed in [14] for Newtonian ferrofluids. If the ramping of N_B goes on [Fig. 5(d)], the growth in the number of fingers continues and a six-fingered limiting shape is obtained for which the fingers tend to pinch off. Incidentally, equivalent pinch-off phenomena have also been found in [14]. The fact that the patterns presented in Fig. 5 tend to the shapes obtained for Newtonian ferrofluids under a radial field makes perfect sense: as N_B is increased the yield stress effects are eventually overcome, making the MR fluid to behave like usual ferrofluids. Note that the linear prediction which regards the growth of a larger number of fingers for increased N_B is consonant with the generic features of the exact solutions illustrated in Fig. 5. Moreover, the weakly nonlinear prediction related to the formation of sharper and sharper fingering structures as N_B is increased can be also verified.

We close this section by discussing an important issue for the relevance of the exact solutions we have found in this work, which refers to their stability. It is known that similar classes of exact solutions, for instance those that arise in the rotating Hele-Shaw problem [40,41], are unstable. Likewise, the exact stationary patterning structures which emerge when a Newtonian ferrofluid droplet is subjected to an applied radial magnetic field [14] are also unstable. To the best of our knowledge the only known stable exact solutions are those related to peculiar shapes presenting cusplike protrusions obtained for rotating Hele-Shaw flows, in the limit of infinitely long filaments [42].

Despite the stabilizing role played by yield stress effects, we have verified that the exact solutions for MR fluids we investigated in this work are in fact unstable. Most situations will not have a steady state attractor so that a direct connection to the linear and weakly nonlinear regimes can be nontrivial. Moreover, it is correct to say that most of the exact stationary shapes found in [14,40–43], and the ones obtained in this work, are of considerable difficulty to be observed experimentally in a direct fashion. In practice, as discussed in [40] in order to obtain such stationary solutions one has to be able to carefully set initial conditions, which should be sufficiently close to these prescribed forms. In the case of magnetic fluids, this question of experimental accessibility of the steady exact solutions could be possibly facilitated by designing a magnet with the desired shape, and using it to set the proper initial condition in a more controlled fashion [44]. Once this situation is achieved one would verify a slowing down of the dynamics in the neighborhood of stationary states. Actually, an analogous line of reasoning has been recently used in [42] where it is argued that exact stationary solutions obtained for the rotating Hele-Shaw problem could be of relevance to explain a transient slowing down observed in existing experiments [45].

V. CONCLUSIONS

The study of Hele-Shaw pattern formation in ferrofluids has been largely explored during the last few decades. These investigations have unveiled a number of patterning structures and interesting dynamic behaviors. However, the same cannot be said about similar studies for confined magnetorheological fluids. In this work we have examined the emergence of patterns in a complex magnetic fluid, in which its yield stress properties can be tuned by an external radial magnetic field.

By using linear analysis, mode-coupling theory, and a vortex-sheet formalism we have been able to identify several features about the stability and morphology of the confined MR fluid patterns. At linear stages of the dynamics, we have found that the yield stress contributions tend to stabilize the interface, restraining the number of fingering structures formed. At the weakly nonlinear level, the yield stress acts to inhibit the formation of highly spiky fingers induced by the applied field. Finally, by assuming a stationary condition we have accessed fully nonlinear shapes, which look like swollen polygons, whose edges undergo a morphological transition by varying from convex to concave structures. Despite their unstable character, this class of exact solutions can provide useful insights for the understanding of some important fully nonlinear aspects of this complex pattern forming system.

ACKNOWLEDGMENTS

J.A.M. and S.A.L. thank CNPq (Brazilian Research Council) for financial support of this research through the program "Instituto Nacional de Ciência e Tecnologia de Fluidos Complexos (INCT-FCx)," and also through the CNPq/FAPESQ Pronex program. R.M.O. wishes to thank CAPES (Brazilian sponsor) and Fullbright for financial support through Grant No. BEX 2615/06-1, IIE ID No. 15073695.

[1] R. E. Rosensweig, *Ferrohydrodynamics* (Cambridge University Press, Cambridge, 1985).
[2] E. Blums, A. Cebers, and M. M. Maiorov, *Magnetic Fluids* (de Gruyter, New York, 1997).
[3] C. Rinaldi, A. Chaves, S. Elborai, X. He, and M. Zahn, Curr. Opin. Colloid Interface Sci. **10**, 141 (2005).
[4] D. Andelman and R. E. Rosensweig, J. Phys. Chem. B **113**, 3785 (2009).
[5] P. G. Saffman and G. I. Taylor, Proc. R. Soc. London, Ser. A **245**, 312 (1958).
[6] For review papers see for instance, G. Homsy, Annu. Rev. Fluid Mech. **19**, 271 (1987); K. V. McCloud and J. V. Maher, Phys. Rep. **260**, 139 (1995); J. Casademunt, Chaos **14**, 809 (2004).
[7] A. O. Tsebers and M. M. Maiorov, Magnetohydrodynamics (N.Y.) **16**, 21 (1980).
[8] D. P. Jackson, R. E. Goldstein, and A. O. Cebers, Phys. Rev. E **50**, 298 (1994).
[9] G. Pacitto, C. Flament, J.-C. Bacri, and M. Widom, Phys. Rev. E **62**, 7941 (2000).
[10] S. Elborai, D.-K. Kim, X. He, S.-H. Lee, S. Rhodes, and M. Zahn, J. Appl. Phys. **97**, 10Q303 (2005).
[11] D. P. Jackson and J. A. Miranda, Phys. Rev. E **67**, 017301 (2003).
[12] D. P. Jackson and J. A. Miranda, Eur. Phys. J. E **23**, 389 (2007).
[13] C.-Y. Chen, S.-Y. Wu, and J. A. Miranda, Phys. Rev. E **75**, 036310 (2007).
[14] R. M. Oliveira, J. A. Miranda, and E. S. G. Leandro, Phys. Rev. E **77**, 016304 (2008).
[15] J. Rabinow, AIEE Trans. **67**, 1308 (1948).
[16] J. M. Ginder, in *Encyclopedia of Applied Physics*, edited by G. L. Trigg (VCH, Weinheim, 1996), Vol. 16, p. 487.
[17] J. M. Ginder, MRS Bull. **23**, 26 (1998).
[18] G. Bossis, S. Lacis, A. Meunier, and O. Volkova, J. Magn. Magn. Mater. **252**, 224 (2002).
[19] S. Genç and P. P. Phulé, Smart Mater. Struct. **11**, 140 (2002).
[20] H. A. Barnes, J. Non-Newtonian Fluid Mech. **81**, 133 (1999).
[21] H. Shahnazian and S. Odenbach, Int. J. Mod. Phys. B **21**, 4806 (2007).
[22] H. Shahnazian and S. Odenbach, J. Phys.: Condens. Matter **20**, 204137 (2008).
[23] C.-Y. Chen, Y.-S. Yang, and J. A. Miranda, Phys. Rev. E **80**, 016314 (2009).
[24] P. Coussot, J. Fluid Mech. **380**, 363 (1999).
[25] G. H. Covey and B. R. Stanmore, J. Non-Newtonian Fluid Mech. **8**, 249 (1981).
[26] S. A. Lira and J. A. Miranda, Phys. Rev. E **80**, 046313 (2009).
[27] R. Ewoldt, Ph.D. thesis, Massachusetts Institute of Technology, 2009.
[28] R. Ewoldt, G. McKinley, and A. Hosoi, Bull. Am. Phys. Soc. **53**(15), 252 (2008).
[29] S. A. Lira and J. A. Miranda, Phys. Rev. E **79**, 046303 (2009).
[30] Ll. Carrillo, F. X. Magdaleno, J. Casademunt, and J. Ortín, Phys. Rev. E **54**, 6260 (1996).
[31] E. Alvarez-Lacalle, E. Pauné, J. Casademunt, and J. Ortín, Phys. Rev. E **68**, 026308 (2003).
[32] H. Gadêlha and J. A. Miranda, Phys. Rev. E **70**, 066308 (2004).
[33] J. A. Miranda and M. Widom, Int. J. Mod. Phys. B **12**, 931 (1998).
[34] E. Alvarez-Lacalle, J. Casademunt, and J. Ortín, Phys. Rev. E **64**, 016302 (2001).
[35] G. Tryggvason and H. Aref, J. Fluid Mech. **136**, 1 (1983).
[36] G. Birkhoff, Los Alamos Scientific Laboratory Technical Report No. LA-1862, 1954 (unpublished).
[37] P. Kuzhir, M. T. López-López, and G. Bossis, Phys. Fluids **21**, 053101 (2009).
[38] P. P. Phulé and J. M. Ginder, Int. J. Mod. Phys. B **13**, 2019 (1999).
[39] J. A. Miranda and M. Widom, Physica D **120**, 315 (1998).
[40] E. Alvarez-Lacalle, J. Ortín, and J. Casademunt, Phys. Rev. Lett. **92**, 054501 (2004).
[41] E. S. G. Leandro, R. M. Oliveira, and J. A. Miranda, Physica D **237**, 652 (2008).
[42] R. Folch, E. Alvarez-Lacalle, J. Ortín, and J. Casademunt, Phys. Rev. E **80**, 056305 (2009).
[43] J. F. Nye, H. W. Lean, and A. N. Wright, Eur. J. Phys. **5**, 73 (1984).
[44] J. White, J. Oakley, M. Anderson, and R. Bonazza, Phys. Rev. E **81**, 026303 (2010).
[45] E. Alvarez-Lacalle, J. Ortín, and J. Casademunt, Phys. Fluids **16**, 908 (2004).